Desalination 582 (2024) 117595

Contents lists available at ScienceDirect

Desalination

journal homepage: www.elsevier.com/locate/desal

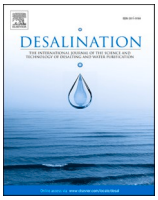

Comparison of current collector architectures for Flow-electrode Capacitive Deionization

Niklas Köller [a], Mila Perrey [a], Lantz K. Brückner [a], Philipp Schäfer [a], Sebastian Werner [a], Christian J. Linnartz [a,b], Matthias Wessling [a,b,*]

[a] RWTH Aachen University, Aachener Verfahrenstechnik-Chemical Process Engineering, Forckenbeckstraße 51, 52074 Aachen, Germany
[b] DWI - Leibniz Institute for Interactive Materials e.V., Forckenbeckstraße 50, 52074 Aachen, Germany

HIGHLIGHTS

- Novel current collector based on bipolar plates made of expanded graphite.
- Comparison of current collector architectures in resistance measurements and FCDI experiments.
- Investigation of flow channel design and length.
- Influence of surface roughness on charge transfer between current collector and flow electrode.

GRAPHICAL ABSTRACT

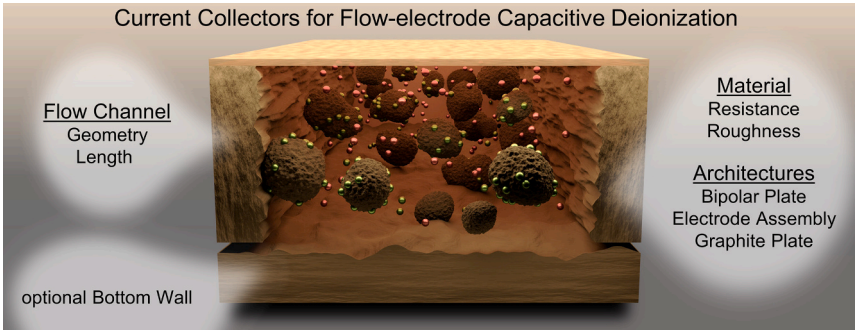

ARTICLE INFO

Keywords:
Flow-electrode capacitive deionization
Desalination
Concentration
Current collector
Membrane-electrode assembly

ABSTRACT

Flow-electrode Capacitive Deionization (FCDI) is a relatively young technology that allows energy-efficient desalination and salt concentration. FCDI employs flow electrodes, suspensions of conductive particles capable of storing ions in the electric double layer at their surface upon charging. To facilitate charging, the flow electrode particles must be electrically contacted using current collectors. Current collectors must guide the flow electrode along a membrane surface, provide a surface area for electrical contact with the particles, and be inert at high salt concentrations. In this study, we compare different current collector architectures for FCDI. Graphite plates and membrane-electrode assemblies made of carbon fiber fabric are two architectures described in the recent literature. We introduce a new current collector architecture based on a bipolar plate made of expanded graphite. These novel current collectors show up to 55 % higher salt transfer than graphite plates, rendering them a valuable new architecture for FCDI modules. Comparative analysis of different current collector architectures shows that the side walls of a flow channel are more effective at charge transport than the bottom wall. Furthermore, surface roughness impacts charge transport, with smoother surfaces leading to higher salt removal rates.

* Corresponding author at: RWTH Aachen University, Aachener Verfahrenstechnik-Chemical Process Engineering, Forckenbeckstraße 51, 52074 Aachen, Germany.
E-mail address: manuscripts.cvt@avt.rwth-aachen.de (M. Wessling).

https://doi.org/10.1016/j.desal.2024.117595
Received 11 January 2024; Received in revised form 28 March 2024; Accepted 28 March 2024
Available online 15 April 2024

1. Introduction

The growth of the human population and global climate change put strain on freshwater resources worldwide. According to projections, 6 out of 10 billion people living on Earth will suffer from scarcity of clean water by 2050 [1,2]. Industrial and agricultural activities further stress the available water resources [3,4]. The wastewater from these processes often contains salts that can harm the water body, even in low concentrations. The aim should be to recycle these wastewaters by desalination and to minimize the amount of water lost. Furthermore, the recycling of valuable salts from wastewater can provide an additional economic incentive [5].

Separation of dissolved salts from water is achieved with different desalination technologies that are either temperature-driven, pressure-driven, or electro-driven. In electro-driven membrane processes, the driving force for ion transport is an electric field, thus eliminating the need for high temperatures and pressures. Studies show that electro-driven membrane processes can be more energy efficient than their alternatives, especially at low salt feed concentrations [6]. The most common process is electrodialysis (ED), in which an alternating array of ion-exchange membranes (IEMs) between two electrodes is used. Research on ED dates back to the 1940s, but improvements in available membranes were necessary to make the process viable and increase the attention it received [7]. IEMs are strongly charged materials that block the passage of salt ions with the same charge [8,9]. Cation-exchange membranes (CEMs) allow the passage of cations while blocking anions from entering the membrane material. Anion-exchange membranes (AEMs) block cations and allow anions to pass. An alternating array of these membranes between two electrodes leads to the formation of diluate and concentrate compartments between the IEMs when an electric field is applied to the electrodes. Electrochemical reactions (mostly water-splitting) at the electrodes drive the ion transport. An ED system can (to some extent) be scaled up by adding more IEMs between the electrodes [10]. The addition of IEMs also adds new resistances to the system, and the voltage at the electrodes needs to be increased to generate the same current as in a system with fewer membranes.

An alternative to ED is Capacitive Deionization (CDI), in which ions are removed from a bulk solution by adsorption to charged electrode surfaces. CDI is enhanced by the addition of IEMs (Membrane CDI, MCDI) to block the adsorption of oppositely charged ions during the regeneration step [11]. Since no electrochemical reactions occur, the process is, in theory, more energy efficient than ED [12]. CDI and MCDI processes can be improved by tailoring the electrode materials to enhance salt adsorption capacity. The development of materials for CDI electrodes is a growing field with notable progress [13]. Common approaches are the use of different carbonaceous materials [14], pseudocapacitive materials such as prussian blue analogues [15–17] or the use of metal-oxide decorated graphite materials [18–23].

(M)CDI has received academic interest and industrial application [24,25]. However, a disadvantage of the technology is its inherently non-continuous operation [13,26].

A continuous MCDI process was made possible in the form of Flow-electrode Capacitive Deionization (FCDI) in 2013 [27]. In this process, a suspension of porous particles is used as a flow electrode, enabling a continuous process with a high capacity for ion adsorption. The particles are charged by contact with static current collectors and by forming charge percolation networks, similar to electrochemical flow capacitors [28–30]. The charged particles then attract ions, which are stored in the electric double layer at the surface of the particles. In early FCDI research, activated carbon particles were used [27,31,32]. In the past ten years, work on flow electrodes has been a significant part of FCDI research [33]. Some researchers focused on a better understanding of charge transfer in flow electrodes through experiments or simulations [30,34–36]. Other researchers investigated different carbon-based materials [37–43] or the modification of flow electrodes with conductive additives (e.g., carbon black). These materials can improve the conductivity and capacity of flow electrodes [44–46]. The charge transfer from the current collectors to the flow electrode particles can also be enhanced with redox active materials in the flow electrodes [47–50]. Intercalation materials and prussian blue analogues have also been used to enhance flow electrodes [51,52].

Simulations show that the contact resistance between the particles and the current collector has a substantial impact on the overall charge transfer resistance [53]. Dennison et al. investigated the effects of channel depth and flow rate on the resistance and conductance of an electrochemical flow capacitor. They found that up to 40 % of cell resistance was caused by fixed resistances of current collectors and interfacial resistance between the current collector and the flow electrode. Thus, they highlighted the interdependence of flow electrode composition and cell design [54]. Wang et al. document charge transfer limitations between the current collector and particles on the anode side of their FCDI cell [55]. Therefore, improvement of current collectors is an important field of FCDI research.

A second rationale for the focus on current collectors is based in the scale-up of FCDI. Initially, FCDI research was done with two modules: one for desalination and the other one for concentration [27,31]. The first step in process intensification and scale-up was the implementation of a single module setup with alternating diluate and concentrate channels [56]. FCDI modules are now designed similarly to ED modules. The main difference is the mechanism of charge transfer in the flow-electrode compartment. ED depends on converting electric current into ion movement by electrochemical reactions. FCDI depends on the contact between the current collector and the flow-electrode particles and the formation of percolation networks. The actual contribution of capacitive storage to ion removal in FCDI is the subject of debate [57,58].

Nevertheless, it is worth exploring the boundaries of the technology with new modules on an increased scale. He et al. demonstrated scale-up with a tubular FCDI module [59]. However, most researchers use plate and frame type modules for scale-up [60,61]. Here, stacking can enable scale-up, similar to ED. In the case of FCDI not only the IEMs need to be stacked but also the current collectors need to be repeated [62]. This renders current collectors similar to bipolar plates used in electrolyzers or fuel cells [63,64]. Since multiple current collectors are needed for module scale-up by stacking, the performance and the price of the current collectors become increasingly important.

Typically, graphite plates act as current collectors in FCDI. They fulfill all requirements: they are electrically conductive, chemically inert in salt solutions, can be easily machined, and are not too expensive. However, they are not well suited for stacking. Graphite is brittle and susceptible to breaking; thus, thick plates are needed to achieve mechanical stability. Furthermore, machining the flow channels does cause significant costs. For these reasons, alternative current collector architectures have been investigated. Xu et al. have used so-called membrane-current collectors (MCCs) which are an assembly of a titanium mesh and an IEM [65,66]. Three-dimensional current collectors based on metal meshes or foams offer higher surface area between current collector and flow electrode particles [67,68]. However, these three-dimensional current collectors were so far not tested in scale-up. Chen et al. have coated regular graphite current collectors with polyaniline to reduce surface roughness and ohmic resistance at the interface between the current collector and the flow electrode [69]. Li et al. have used additional carbon felts in their modules and achieved a 63 % increase in salt removal rate [70]. Recently, Saif et al. used 3D-printed gaskets to form a flow channel on top of a Pt-coated titanium current collector [71]. In the past, our group has developed membrane-electrode assemblies (MEAs), in which the IEM is hotpressed to a carbon fiber fabric (CFF) [72]. In this case, the membrane and the current collector form a single part, with the CFF acting as functional reinforcement. Thus, thinner membranes could be used. Since the MEAs do not feature a flow channel for the flow electrode, a second part (usually 3D-printed from a polymeric, non-conductive material) is necessary.

Notably, MCCs and MEAs also change the concept of charge transfer from the current collector to the particles in the flow electrode. Charge transfer no longer occurs at the three walls of the flow channel but directly at the membrane. Although this leads to a significantly smaller area for electron exchange with the flow electrode, the salt transport rate remains constant. We hypothesized that this was due to shorter transfer paths in the MEA [72]. However, we were unable to prove this hypothesis; this is the first reason we revisit the topic of current collectors. The second reason is the MEA manufacturing process. Although MEAs allow the scale-up of FCDI modules [62], their production is labor- and time-intensive. The hotpressing step is followed by a sealing step with silicone rubber. Additionally, a second part is needed to provide the flow channel. New current collector architectures should aim to reduce the number of parts and manufacturing steps.

Bipolar plate (BP) current collectors from expanded graphite, used in some fuel cells or redox-flow batteries [73], offer a viable alternative. Expanded graphite plates are available in thicknesses up to 2 mm. Thus, cutting of a flow channel for a flow electrode is possible. In addition, assemblies of current collector and IEM can be formed by hotpressing an IEM to the expanded graphite. This facilitates easy production of BP current collectors: the only steps necessary are cutting of the flow channel and hotpressing; no further gaskets or sealing steps are necessary. An overview of the manufacturing steps for the current collector architectures investigated in this work is given in Table 1. More detail on the advantages and disadvantages of the manufacturing processes is given in the Supplementary Information.

Composite expanded graphite plates with around 10 % of polymeric binder are more durable than those made from pure graphite. This renders them better suited for the manufacturing of BPs. The flow channel can be cut with a waterjet cutter. This generates a flow channel in which the two walls provide the area for charge transport, as shown in Fig. 1. With the graphite plates, MEAs, and BPs, there are three different current collector architectures that utilize different materials and have varying interfacial areas for charge transport to the flow-electrode particles. This works aims to compare these current collector architectures in FCDI experiments. We hypothesize that the surface area between the current collector and the flow electrode influences the performance of different current collector architectures. This surface facilitates the transport of electrons between the current collectors and the flow electrode particles. In the following, the surface area is referred to as electron transfer area (ETA). Furthermore, the influence of surface roughness is investigated.

2. Experimental

2.1. Characterization of current collector materials

In this study, three different current collector architectures are compared. The first step was to characterize the different materials in electrical resistance measurements. Samples of the materials (50 mm × 50 mm) were clamped between copper plates in a press with a force of 97 kN at a temperature of 25 °C. Chronoamperometric measurements with a voltage of 1 mV were used to determine ohmic resistances, and the resistances of the copper plates were deducted. The average resistances of three experiments were used for the comparison. From these results, resistivities were calculated according to Eq. (1). Here ρ is the material-specific resistivity, R is the measured resistance, A_{cond} is the surface area in contact with the copper plate, and l_{cond} is the thickness of the sample.

$$\rho = R \cdot \frac{A_{cond}}{l_{cond}} \quad (1)$$

Table 1
Manufacturing steps for the flow channel, the membrane and the sealings needed for the different current collector architectures.

Architecture	Graphite Plate	MEA	Bipolar Plate
Flow channel	Milling	3D-printing	Waterjet-cutting
Membrane treatment	Untreated	Hotpressing	Hotpressing
Sealings	Gaskets	Silicone	Not necessary

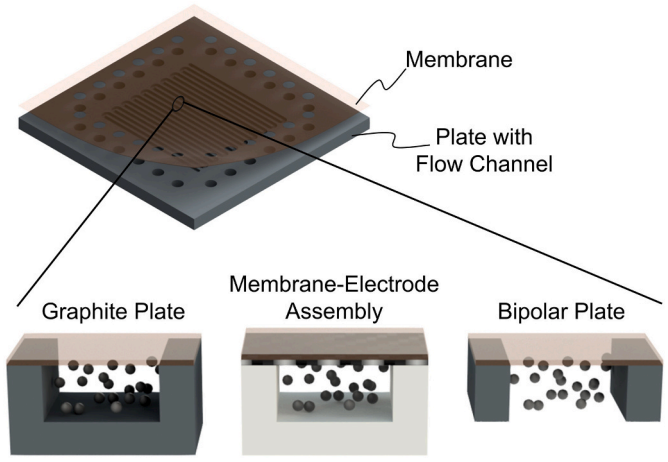

Fig. 1. Difference in the investigated FCDI architectures. When using a graphite plate, charge transfer between the current collector and flow electrode can occur at three channel walls shown in grey. For the MEA this reduces to the surface area of the carbon fiber fabric beneath the membrane and for the bipolar plate to the two side walls.

Graphite plates are commonly used in FCDI research, and MEAs were investigated in a previous study [72]. Bipolar plates (BPs) made from expanded graphite are a new approach in FCDI; therefore, the material was investigated with XRD (Empyrean Series 2, Malvern Panalytical Ltd.) and compared to the graphite plates. The surface roughnesses of the current collectors were investigated by field emission scanning electron microscopy (FE-SEM SU5000, Hitachi High-Tech Corporation) and optical profilometry (NT2000, Wyko Corporation). Furthermore, the attachment of the membrane to the bipolar plate was investigated by swelling tests and field emission scanning electron microscopy.

2.2. Manufacturing of current collectors for FCDI experiments

FCDI modules were built as single modules [56,74] with ED-100 membranes (active membrane area A_{mem} = 100 cm^2, Fumatech BWT GmbH). One module consisted of two current collectors (one positively and one negatively contacted). First, graphite plate (GP) current collectors and MEAs were compared with BPs with fixed geometry. Then, the geometry of BPs was varied. The epoxy-impregnated GPs (180 × 180 × 10 mm, MR40, Müller & Rössner GmbH & Co. KG) have meandering flow channels with 14 turns milled into one side for the flow electrodes (3 mm × 1.45 mm and 1556 mm total length). The same flow channel layout is also used in the MEA and BP modules, as shown in Fig. 2 (a). In the flow channel cross-sections, the conductive material is shown in grey and the non-conductive material in white. The resulting electron transfer area (ETA) for each architecture is given.

In the next step, the channel lengths of the BP current collectors were varied by reducing the number of turns of the meander channel from 14 to 10 and to 6, as shown in Fig. 2 (b). Another set of experiments (shown in Fig. 2 c) investigated the influence of the channel side walls and the bottom wall. The BP geometry with 14 turns was used. The side walls were replaced by non-conductive polymeric material and a second BP without flow channel geometry was added as the bottom wall.

MEAs were manufactured with 30 µm thick FKS-30 (Fumatech BWT GmbH) membranes, according to the process described by Linnartz et al. [72]. Furthermore, a 10 mm rim at the edges of the MEAs was fitted with copper tape with a conductive adhesive (ET1181, 3 M Corporation) to enable good electrical contact. The flow fields for the MEA modules

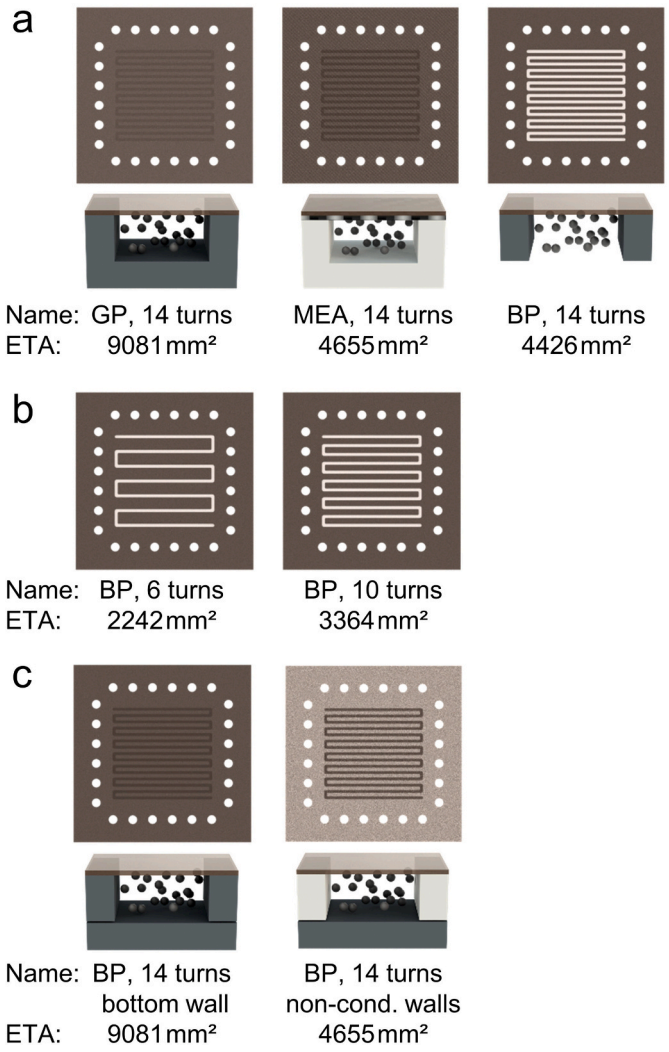

Fig. 2. FCDI current collectors investigated in this study. (a): Comparison of different architectures. The GP and the MEA architecture consist of two separate parts, in the BP architecture the membrane and current collector form an assembly. The flow channel geometry is the same in all three architectures. (b): BP architectures with shorter flow channels, leading to lower electron transfer area (ETA). (c): BP architectures with the addition of a conductive bottom wall. The BP with a conductive bottom wall has the same ETA as the GP architecture. The conductive bottom wall with non-conductive side walls has the same ETA as the MEA architecture.

were 3D-printed (printer: Objet Eden260, material: VeroClear, Stratasys Ltd.). For the BP modules, expanded graphite plates (Sigracell® FR10, SGL Carbon SE) with a thickness of 1.6 mm were used. The flow channel was cut into the plates by waterjet cutting. Then CEMs (FKS-130, Fumatech BWT GmbH) were pressed onto the plates at 120 °C and 570 N/cm^2 for 7 min. During pressing, the plate and the CEM were placed between aluminum plates (to achieve a good alignment of the CEM) and 250 µm thick sheets of PTFE (to avoid sticking of the CEM to the aluminum plate). The edges of the BP current collectors were also fitted with the same copper tape. The pressing procedure caused the thickness of the expanded graphite plate to reduce to 1.45 mm. Thus, the same channel depth was used for the manufacturing of the flow fields for MEAs and GPs. Anion exchange membranes (FAS-130, Fumatech BWT GmbH) and two 470 µm thick mesh spacers (ED-100 Spacer, Deukum GmbH) were used to complete the modules. Polyoxymethylene end plates were used to clamp the modules and provide connections for the flow-electrode channels and the feed spacers.

2.3. FCDI experiments

FCDI experiments were carried out in continuous single-pass operation. Feed solutions were prepared by dissolving 60 g/L sodium chloride (VWR International GmbH) in ultrapure water. The flow electrode was prepared by suspending 15 wt% activated carbon powder (Carbopal SC11PG, Donau Carbon GmbH) in the same solution. The flow electrode was stirred for at least 12 h prior to use. The water feed flows were conveyed by peristaltic pumps (REGLO ICC Digital Peristaltic Pump 2-Channel, Cole-Parmer Instrument Company Ltd.) from a feed vessel through the module to a product vessel. The flow electrode was conveyed with a peristaltic pump (Masterflex Easyload II, Cole-Parmer Instrument Company Ltd.), and the flow rate was set to 200 mL/min for all experiments. The electric potential was provided to the module by a power supply, which also measured the current (HM8143, Rohde & Schwarz GmbH & Co. KG). Conductivities of diluate and concentrate at the module outlet were measured with conductivity sensors (SE615-MS, Knick Elektronische Messgeräte GmbH & Co. KG and LTC0.35/23, Xylem Analytics Germany Sales GmbH & Co. KG). Data from the conductivity sensors and the power supply were logged with a setup supplied by ZUMOLab GmbH. Due to the single-pass experiment mode, the outlet conductivities develop to a steady state. This steady state was used to compare the experiments with each other. The inlet and outlet mass flows were measured by taking samples for a constant duration of 20 min during steady state and weighing them. The density of the samples was measured (Densito 30PX, Mettler-Toledo International Inc.), allowing the calculation of exact volumetric flow rates. A correlation between density and sodium chloride (NaCl) concentration (see Supplementary Information Fig. S4) was used to calculate concentrations from the measured density. The validity of this correlation was verified by investigating some samples with ion chromatography (930 Compact IC Flex, Deutsche METROHM GmbH & Co. KG. Anion column: Metrosep A Supp 7 - 250/4.0. Cation column: Metrosep C 6 - 250/4.0). The deviation between the ion chromatography results and the correlation results was in the range of ±5%. For each different FCDI module, at least three experiments were performed and included in the evaluation.

2.4. Metrics used in FCDI experiments

The experiments are evaluated by comparing the concentration differences between diluate and concentrate. Concentrations are normalized by dividing by the feed concentration c_F. Furthermore, the current efficiency (*CE*, Eq. (2)) and the average salt transfer rate (*ASTR*, Eq. (3)) are calculated. CE is calculated with $z_{NaCl} = 1$, Faraday's constant F, and the molar mass of sodium chloride M_{NaCl}. The current I is the average current during the sampling time. The salt mass flux $\Delta\dot{m}_{NaCl}$ is calculated using a mass balance around the concentrate or diluate channels. These mass balances are decoupled from each other by the flow-electrode compartment, which leads to slight variations between the independent mass balances. Thus, individual CEs for diluate and concentrate are calculated and averaged. The averaged CEs are used to compare the different modules. The same procedure is applied to calculate the ASTR. The average salt mass flux is divided by the active membrane area installed in the modules $A_{Mem,tot} = 300$ cm^2 (from two 100 cm^2 CEMs and one 100 cm^2 AEM) which is constant in all experiments and the molar mass of sodium chloride M_{NaCl}.

$$CE = \frac{z_{NaCl} \cdot F \cdot \Delta\dot{m}_{NaCl}}{I \cdot M_{NaCl}} \tag{2}$$

$$ASTR = \frac{\Delta\dot{m}_{NaCl}}{A_{Mem,tot} \cdot M_{NaCl}} \tag{3}$$

3. Results and discussion

While different current collector designs for FCDI are known in the literature, to the best of our knowledge, there are no studies in which bipolar plates (BPs) made of expanded graphite are used. Thus, initial tests were necessary to evaluate the material and compare it to reference materials. XRD was used to compare the material to pure graphite and expanded graphite without binder material. The measurements show no structural differences between the three materials; the results are given in Supplementary Information Fig. S1.

Electrical resistances of BP material were compared to those of a graphite plate and carbon fiber fabric used for membrane-electrode assemblies (MEAs). Low resistances are an important prerequisite for current collectors. Graphite is an anisotropic material with a difference between in-plane and through-plane resistances. Expanded graphite also shows this anisotropy at the macroscopic level [75]. According to the manufacturer's datasheet, the through-plane resistivity of the bipolar plates is higher (in-plane: $7 \times 10^{-6}\,\Omega\cdot m$, through-plane: $1 \times 10^{-3}\,\Omega\cdot m$). Thus, through-plane measurements were used to compare the materials. All materials were tested in the thicknesses that were used to manufacture current collectors for FCDI experiments (graphite plate 10 mm, BP 1.6 mm, MEA 0.1 mm). First, the electrical resistances of the material samples were measured, then resistivities were calculated according to Eq. (1) to enable comparison with data reported in other research. The bipolar plates used in our study contain a polymeric binder. The influence of the binder material on the resistance is investigated by measuring a sample of pure expanded graphite as comparison. The resistances are shown in Fig. 3. The values range from 0.36 $m\Omega$ for the carbon fiber fabric used in MEAs to 0.52 $m\Omega$ for the BP. Notably, the resistance of the pure expanded graphite is higher than that of the BP. However, the differences between the materials are negligible in comparison to the typical ohmic resistances of an FCDI cell (800 $m\Omega$). Additionally, resistivities are shown in Fig. 3. The resistivity of the bipolar plate is $8 \times 10^{-4}\,\Omega\cdot m$, close to the manufacturer's value of $1 \times 10^{-3}\,\Omega\cdot m$.

The results of the hotpressing of BPs are investigated by field emission scanning electron microscopy. The images in Fig. 4 (a) and (b) show that the ion exchange membrane only adheres to the top layer of the expanded graphite and does not penetrate the material. At the edges, the membrane detaches slightly from the expanded graphite. However, the connection of the two materials is stable enough to withstand handling without any issues. Swelling of the membrane in water also does not cause delamination, as shown in the photographs in Fig. 4 (c) and (d). A sample cut from a BP was photographed first in the dry state (c) and then again after being submerged in ultrapure water for seven days (d). Although local delamination of the membrane and the expanded graphite is visible as light spots, the membrane remained firmly attached. In the FCDI experiments, the BPs are clamped in the FCDI modules. When these modules were taken apart after the experiments, no delamination of the membranes from the expanded graphite plates was observed.

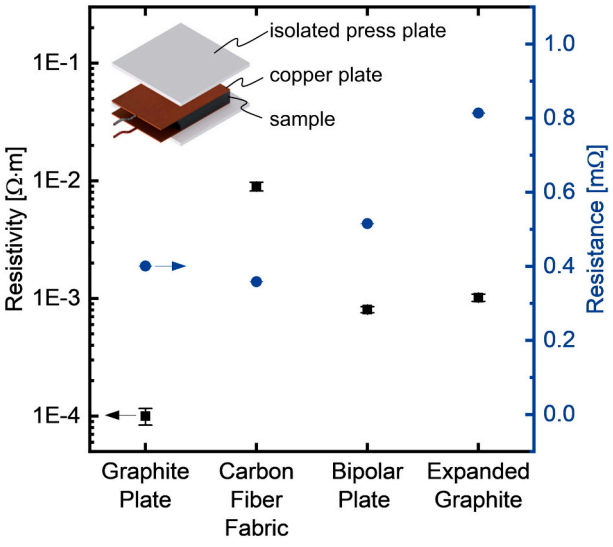

Fig. 3. Resistivities and resistances of different materials studied as FCDI current collectors. The resistance of the bipolar plate is compared to graphite, carbon fiber fabric used for MEAs and a plate of pure expanded graphite.

3.1. FCDI experiments

FCDI experiments were performed to compare the different current collector architectures. In the first set of experiments, newly developed BPs were compared with graphite plates (GPs) and membrane-electrode assemblies (MEAs). The arrangement of ion-exchange membranes in all architectures was CEM-AEM-CEM. For the BP architecture, a comparison between CEM-AEM-CEM and AEM-CEM-AEM is given in Supplementary Information Fig. S5.

Fig. 5 (a) shows the concentration differences reached in the experiments. GP and BP architectures show higher concentration differences in the diluate and concentrate as the MEA architecture. Fig. 5 (b) shows high current efficiencies above 0.95 for all architectures. Small and unavoidable errors in the measurement of flow rates and concentrations strongly influence current efficiencies. A detailed analysis of these errors is given in the Supplementary Information. These errors render the absolute value of the current efficiencies less reliable. However, it can be concluded that all three architectures exhibit high current efficiencies, suggesting that no electrochemical reactions occur. The average salt transfer rate (ASTR) of the BP architecture is higher than that of GPs and MEAs. BPs also have the advantages of being thinner and easier to manufacture. Interestingly, the larger electron transfer area (ETA) of the GPs (shown in Fig. 2) does not influence the results. This result is in line with the results obtained from the study of MEAs [72]. In that study, it was hypothesized that the close contact between the current collector and membrane in the MEAs was the reason for the similar performance. Since there is no such close contact in the BP architecture, we became interested in the influence of current collector designs on the ASTR. Our goal is not to investigate the charge transport at the microscopical level but to develop rules for the design of current collectors that enhance the salt transport in FCDI.

When flow-electrode composition, membranes, and operating voltage are kept constant, there are four parameters of the current collectors that can influence charge transport in FCDI: membrane area, electron transfer area, flow channel design (hydrodynamics), and current collector material. When altering current collector designs, it is difficult to vary one of the parameters independently from the others. In the first step, we deliberately shortened the flow channels of the BPs from 14 turns to 10 and 6 turns. By doing so, we reduced the electron transfer area, and the membrane area between the spacer channels and the flow electrode. Notably, the waterjet cutting enables an easy and quick manufacturing of the different geometries. The resulting designs are shown in Fig. 2 (b).

Since the flow rate of the flow electrode and the depth and width of the channels were kept constant, shorter flow channels lead to lower pressure drops (see Supplementary Information Fig. S7). We never encountered problems with flow-electrode clogging; hence, we assume that the altered pressure drop does not influence the results. Thus, the only parameters that varied were the membrane area and the ETA. The results of the experiments are shown in Fig. 6. Here, concentration differences and ASTR are plotted over the ETA. The ETA is defined as the sum of all conductive surface areas, where flow-electrode particles can exchange charge with the current collectors. The current efficiency of the experiments is given to demonstrate that the experiments are not influenced by low efficiency. As mentioned above, it is important to

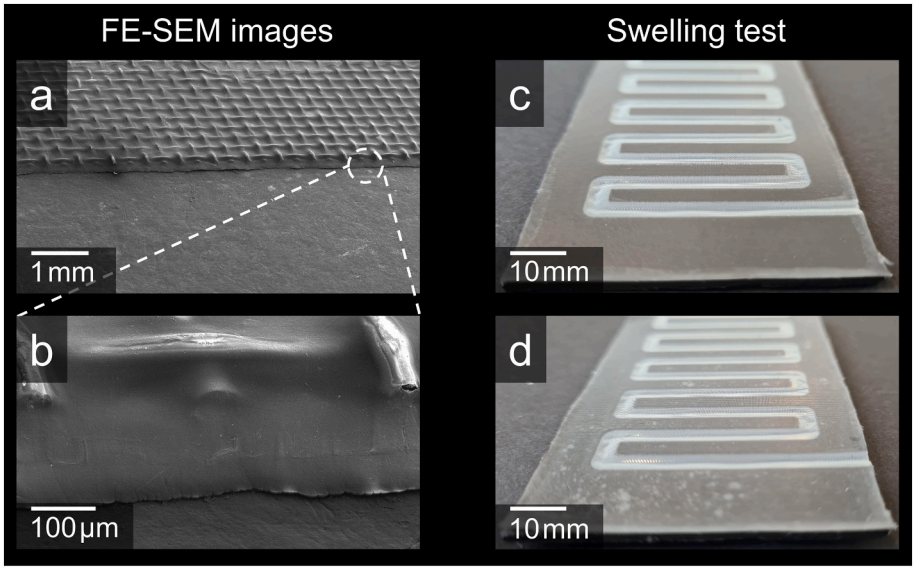

Fig. 4. Visual investigation of BPs. (a) and (b) show FE-SEM images of the membrane hotpressed to the expanded graphite plate. (c) and (d) show photographs of a different sample that was used to investigate membrane swelling in ultrapure water. After seven days some light spots are visible, that show local delamination of the membrane. Overall, the membrane remained firmly attached.

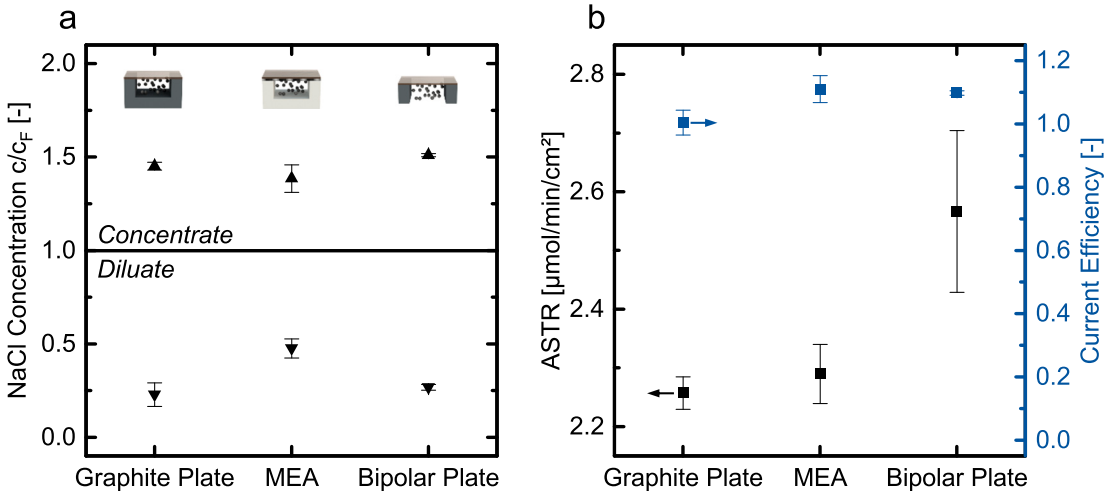

Fig. 5. Results of FCDI experiments with the different current collector architectures investigated in this study. The feed flow rates of the diluate and concentrate were kept constant at 1 mL/min, the voltage at the modules was set to 1.2 V.

handle the absolute values of the current efficiency with caution. However, by comparing the values obtained from various experiments, it can be concluded that none of the experiments are constrained by a significantly lowered current efficiency. The concentration differences and the ASTR show almost linear behavior. The same is true for plotting these metrics over the membrane area since the membrane area and the ETA are geometrically linked to each other (see Supplementary Information Fig. S6 for a plot of the concentration difference and ASTR over the membrane area).

From these experiments, it can be concluded that the length of the flow channel in a current collector influences the salt transfer in FCDI. This could be due to the influence of the membrane area, ETA, or both. We assume that the membrane area is not a limiting factor for ion transport, as current densities in all experiments are around 25 mA/cm^2, and ion-exchange membranes can be operated with current densities up to 50 mA/cm^2 in electrodialysis [76,77]. This implies that the lower ETA is responsible for the lower ASTR. Future current collector design should aim to maximize both the membrane area and the ETA. As shown here, this is possible by adding more turns to a meandering flow channel. However, the number of turns is limited by the width of the corrugations forming the flow channel. With the BP material used here, a minimum width of 3 mm is required to guarantee mechanical stability. Alternatively, the width of the flow channels could be minimized to achieve a higher number of turns in the same area. However, this would change the hydrodynamics of the flow electrode in the channel. Innovative designs for flow channels given in literature could be used for BP current collectors in future [78–80].

In the next step, we wanted to test the effect of varying the ETA without influencing the membrane area. An easy way to do this is to add a backplate made of conductive material to the initial BP setup. In this case, we used a plate cut from the stock material of our BPs without a flow channel. When the plates are pressed together in the FCDI module, a seal is formed between them without the need for gaskets. While our standard BP module has an ETA of 4426 mm^2, the system with the bottom wall has an ETA of 9081 mm^2, same as the graphite plate architecture. In addition to the experiments with the bottom wall, we also

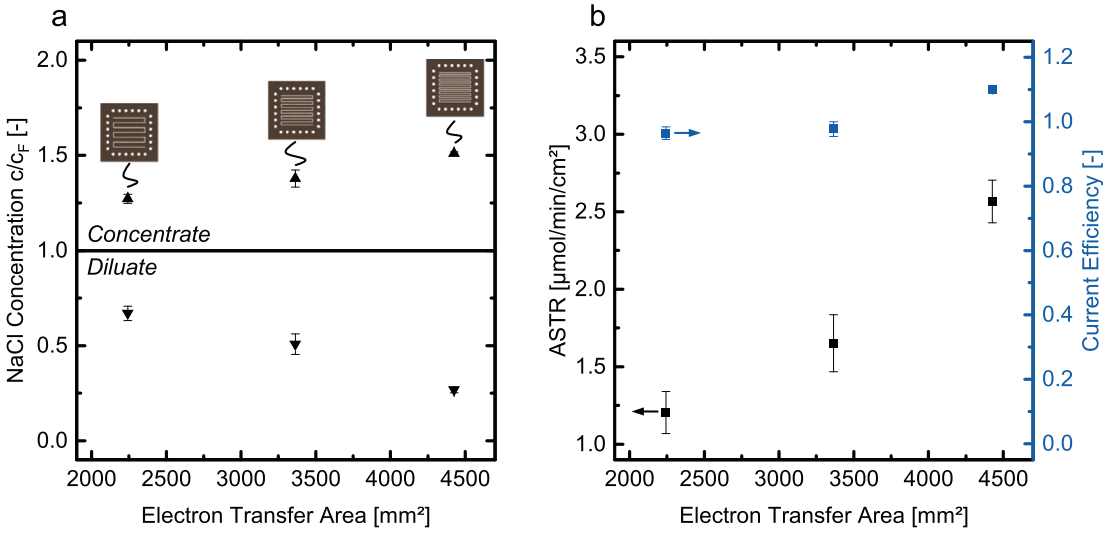

Fig. 6. Impact of flow channel length on desalination experiments with BP architecture.

investigated a system with a conductive bottom wall but non-conductive side walls. In this case, the side walls of the flow channel were made of polymeric material. This led to an ETA of 4655 mm^2, same as the MEA architecture. However, the flow channel cross-section and the membrane area remain unchanged. The flow channel geometries are shown in Fig. 2 (c).

The concentration differences depicted in Fig. 7 (a) show no significant differences between the standard BP and the conductive bottom wall with non-conductive side walls. However, adding the bottom wall to the BP leads to a higher concentration difference. While the BP without a bottom wall achieves a diluate concentration of $0.27\,c_F$ and a concentration of $1.51\,c_F$ the system with the bottom wall reaches $0.02\,c_F$ and $1.61\,c_F$. This is by far the largest concentration difference documented in our experiments and comes close to the complete removal of salt from the diluate feed. Fig. 7 (b) shows high current efficiencies for all three modules. Non-conductive side walls give a lower ASTR than the standard BP, although the ETA is higher. This result suggests that charging the flow-electrode particles at the side walls is more effective. Interestingly, the ASTR is almost equal to the result from the MEA architecture shown in Fig. 5 (b). For both sets of experiments, the average ASTR is 2.29 $\mu mol/(min \cdot cm^2)$. This is consistent with expectations since both systems have the same ETA. Therefore, the results suggest no difference between charging the particles at the bottom of the flow channel or at the top close to the membrane. Further investigation in future work is required, as it can aid in the design of flow channels for FCDI or similar processes.

The BP with the bottom wall has an ETA of 9081 mm^2 and reaches a current density of 34 mA/cm^2 and the highest ASTR (3.55 $\mu mol/(min \cdot cm^2)$). However, the ASTR is lower than the ASTRs of the other two modules in this comparison added together. A possible cause are the low diluate concentrations reached in these experiments. Single-pass experiments lead to low diluate concentrations towards the outlet of the FCDI module. In this case, the diluate concentrations reach 1.75 g/L. Thus, there is insufficient salt left to be transported, limiting the ASTR. The direct comparison between the graphite plate and the BP with the bottom wall reveals a major disadvantage of the graphite plate architecture. Although both have an ETA of 9081 mm^2, the ASTR when using the BP is 55 % higher. Differences in hydrodynamics, membrane area, or ETA cannot explain this result. Therefore, it must be caused by differences in the materials. Chen et al. hypothesized that charge transfer of graphite plates can be hindered by surface roughness and oxygen erosion of the carbon microcrystals at the surface of the graphite.

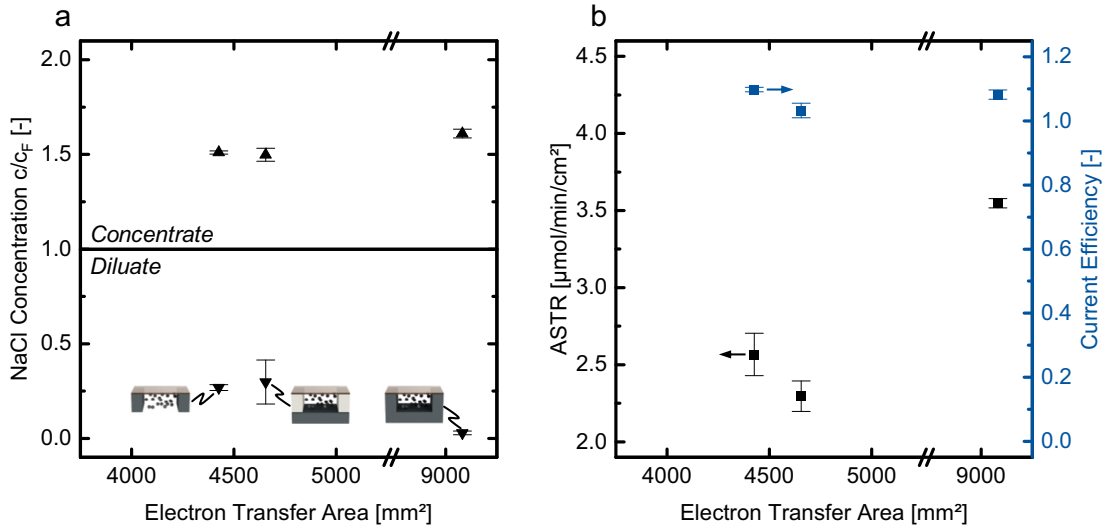

Fig. 7. Results of desalination experiments with bipolar plates, conductive bottom walls and non-conductive side walls.

They were able to improve their graphite current collectors by coating them with polyaniline [69]. Surface roughness is also a possible cause in our experiments because of the different materials and manufacturing techniques we used to obtain the current collectors.

The difference in surface quality is investigated with field emission scanning microscopy (FE-SEM) and optical profilometry. FE-SEM images are shown in Fig. 8. The roughness values R_a beneath the images are calculated from profilometry results. The average of at least three measurements at different locations of the material is used. The surface height plots of the profilometry measurements are given in Supplementary Information Fig. S9. The untreated surface of the expanded graphite plate used as the bottom wall (see Fig. 8 c) is the smoothest surface in the comparison. The walls of the channel in the graphite current collector are manufactured by milling and are also relatively smooth (see Fig. 8 a). Here, the side wall is shown, but there is no difference in the smoothness between the side wall and the bottom wall for this current collector (a FE-SEM image showing both the side wall and bottom wall is given in Supplementary Information Fig. S8). The side walls of the BP are significantly rougher than the surface because they are cut with the waterjet cutter. The result of this comparison is inconclusive. The bipolar plate bottom wall is smoother than the graphite plate, but the side walls are less smooth. To investigate whether surface roughness impacts the FCDI experiments, the roughness of the bottom wall is increased. Fig. 8 (d) shows the surface of the bottom wall after artificially increasing the roughness by treatment with sandpaper.

The impact of this artificial surface roughness on ASTR in FCDI experiments is shown in Fig. 9. With a rougher surface of the bottom wall, the ASTR decreases while the current efficiency remains high. However, the ASTR is still more than 40 % higher than for the graphite plate. This result supports our hypothesis that surface roughness influences current collector performance. Future research is needed to understand how surface roughness interferes with the charge transport between the current collectors and the flow-electrode particles. The roughness of the side walls needs to be included in the investigation. Additionally, long-term experiments are needed to test whether the abrasion caused by the flow-electrode particles will deteriorate the surface quality of the BPs and decrease ASTRs over time.

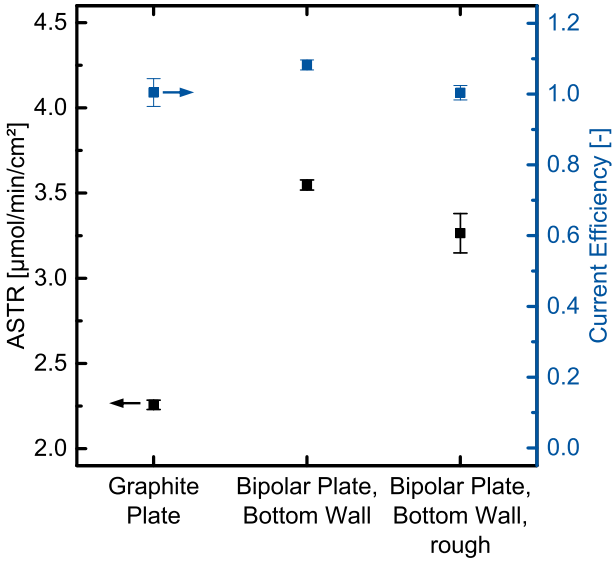

Fig. 9. Results from experiments in which the surface roughness of the bottom wall of the bipolar plate setup is increased. The results from the graphite plate setup are given for reference.

Typically used graphite plate current collectors show a salt transport lower than modules with membrane-electrode assemblies or BPs. The surface roughness of the graphite plates stems from the machining process and could be avoided with a different manufacturing process or a coating. However, graphite plates are likely to remain more expensive

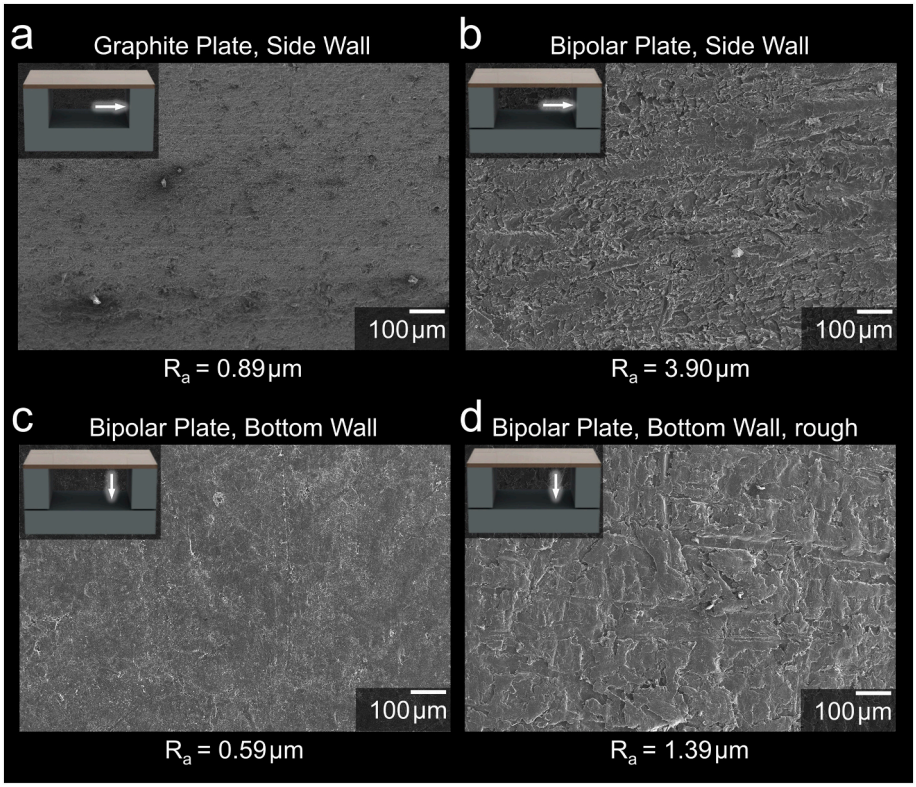

Fig. 8. FE-SEM images of the surfaces of different current collectors. The arrows in the current collector symbols indicate the surfaces shown in the images. The surface roughness values R_a are measured with optical profilometry.

and less well suited for scale-up by stacking.

Our work shows that there is untapped potential for improving FCDI current collectors. Although charge transport between current collectors and flow-electrode particles remains a challenging topic, simple constructive changes in current collectors can lead to important benefits in the FCDI process.

4. Conclusion

Flow-electrode Capacitive Deionization (FCDI) is an innovative technology for the desalination and concentration of water with ion-exchange membranes. FCDI is similar to electrodialysis (ED) and can be scaled up by stacking. Multiple current collectors are necessary to build a stacked FCDI module. Thus, the performance and cost of these current collectors become increasingly important. In this study, we compare different architectures that can be used as current collectors: graphite plates, which are typically used in FCDI research, membrane-electrode assemblies made from carbon fiber fabric, and a new type of bipolar plates made from expanded graphite. Our results show superior salt transport of the bipolar plates, which are also cheaper to manufacture than graphite plates and easier to apply than membrane-electrode assemblies.

The bipolar plates can be used with an ion-exchange membrane on both sides to enable stacking. Alternatively, it is possible to add a conductive bottom wall. With the bottom wall, the surface area where charge can be transported between the current collector and the flow electrode is equal to that of the graphite plate architecture. However, the salt transfer rate with bipolar plates is 55 % higher. We conclude that this enhancement is partially caused by the lower surface roughness of the bottom wall.

Our research shows that the ideal two-dimensional current collector for FCDI with an activated carbon flow electrode must have a high surface area available for charge transport, with the side walls contributing more to the charge transport than the bottom wall. The surfaces should be smooth; however, the influence of surface roughness on charge transfer needs to be investigated in more depth in the future.

Although there is plenty of research on the particles that form the flow electrodes, our work showcases great potential for improvement in the engineering of current collectors. Future studies on FCDI should consider replacing typically used graphite plates with improved current collectors like the bipolar plates presented in this work. Furthermore, current collectors and flow electrodes could be tuned together to optimize charge transfer.

CRediT authorship contribution statement

Niklas Köller: Writing – review & editing, Writing – original draft, Visualization, Validation, Supervision, Project administration, Methodology, Investigation, Formal analysis, Data curation, Conceptualization. **Mila Perrey:** Visualization, Investigation, Data curation. **Lantz K. Brückner:** Data curation, Investigation, Visualization. **Philipp Schäfer:** Data curation, Investigation, Visualization. **Sebastian Werner:** Data curation, Investigation, Visualization. **Christian J. Linnartz:** Conceptualization, Data curation, Formal analysis, Funding acquisition, Methodology, Project administration, Supervision, Validation, Visualization, Writing – original draft, Writing – review & editing. **Matthias Wessling:** Conceptualization, Funding acquisition, Methodology, Project administration, Resources, Supervision, Visualization, Writing – original draft, Writing – review & editing.

Declaration of competing interest

The authors declare that they have no known competing financial interests or personal relationships that could have appeared to influence the work reported in this paper.

Data availability

Data will be made available on request.

Acknowledgments

This work was supported by the German Federal Ministry of Education and Research (BMBF) under the projects “NITREB” (FKZ 02WQ1534D) and “RIKovery” (FKZ 02WV1569). M.W. acknowledges DFG funding through the Gottfried Wilhelm Leibniz Award 2019, Germany (WE 4678/12-1). M. W. appreciates the support from the Alexander-von-Humboldt foundation. This work was enabled by a Bruker SkyScan 1272 funded by the Major Research Instrumentation Programme (DFG-Gz: INST 2221157-1 FUGB) as per Art. 91b GG in the Research Building NW1481006 “NGP2 – Center for Next Generation Processes and Products”. This work was performed in part at the Center for Chemical Polymer Technology CPT, which is supported by the EU and the federal state of North Rhine-Westphalia (grant no. EFRE 30 00 883 02).

The authors thank Justin Gottfried and Timo Linzenmeier for IC measurements, Karin Faensen for µCT and FE-SEM images, Tamás Haraszti for XRD measurements, and Ahmed Mourran for his help with optical profilometry.

Appendix A. Supplementary data

Supplementary data to this article can be found online at https://doi.org/10.1016/j.desal.2024.117595.

References

[1] M.M. Mekonnen, A.Y. Hoekstra, Four billion people facing severe water scarcity, Sci. Adv. 2 (2) (2016) e1500323, https://doi.org/10.1126/sciadv.1500323.
[2] A. Boretti, L. Rosa, Reassessing the projections of the world water development report, npj Clean Water 2 (15) (2019), https://doi.org/10.1038/s41545-019-0039-9.
[3] M.A. Shannon, P.W. Bohn, M. Elimelech, J.G. Georgiadis, B.J. Marin, A.M. Mayes, Science and technology for water purification in the coming decades, Nature 452 (2008) 301–310, https://doi.org/10.1038/nature06599.
[4] M. Cañedo-Argüelles, B.J. Kefford, C. Piscart, N. Prat, R.B. Schäfer, C.-J. Schulz, Salinisation of rivers: an urgent ecological issue, Environ. Pollut. 173 (2013) 157–167, https://doi.org/10.1016/j.envpol.2012.10.011.
[5] T. Tong, M. Elimelech, The global rise of zero liquid discharge for wastewater management: drivers, technologies, and future directions, Environ. Sci. and Technol. 50 (2016) 6846–6855, https://doi.org/10.1021/acs.est.6b01000.
[6] M.M. Generous, N.A. Qasem, U.A. Akbar, S.M. Zubair, Techno-economic assessment of electrodialysis and reverse osmosis desalination plants, Sep. Purif. Technol. 272 (2021) 118875, https://doi.org/10.1016/j.seppur.2021.118875.
[7] H. Strathmann, Chapter 6 Electrodialysis and related processes, in: Membrane Separations Technology - Principles and Applications vol. 2, of Membrane Science and Technology, Elsevier, 1995, pp. 213–281, https://doi.org/10.1016/S0927-5193(06)80008-2.
[8] H. Strathmann, Electrodialysis, a mature technology with a multitude of new applications, Desalination 264 (3) (2010) 268–288, https://doi.org/10.1016/j.desal.2010.04.069.
[9] K. Elsaid, M. Kamil, E.T. Sayed, M.A. Abdelkareem, T. Wilberforce, A. Olabi, Environmental impact of desalination technologies: a review, Sci. Total Environ. 748 (2020) 141528, https://doi.org/10.1016/j.scitotenv.2020.141528.
[10] T. Melin, R. Rautenbach, Membranverfahren: Grundlagen der Modul- und Anlagenauslegung, 3rd edition, Springer-Verlag, Berlin, Heidelberg, 2007, https://doi.org/10.1007/978-3-540-34328-8. VDI-Buch,.
[11] J.-B. Lee, K.-K. Park, H.-M. Eum, C.-W. Lee, Desalination of a thermal power plant wastewater by membrane capacitive deionization, Desalination 196 (1) (2006) 125–134, https://doi.org/10.1016/j.desal.2006.01.011.
[12] S. Porada, R. Zhao, A. van der Wal, V. Presser, P.M. Biesheuvel, Review on the science and technology of water desalination by capacitive deionization, Prog. Mater. Sci. 58 (8) (2013) 1388–1442, https://doi.org/10.1016/j.pmatsci.2013.03.005.
[13] X. Zhao, H. Wei, H. Zhao, Y. Wang, N. Tang, Electrode materials for capacitive deionization: a review, J. Electroanal. Chem. 873 (2020) 114416, https://doi.org/10.1016/j.jelechem.2020.114416.
[14] Z.-H. Huang, Z. Yang, F. Kang, M. Inagaki, Carbon electrodes for capacitive deionization, J. Mater. Chem. A 5 (2017) 470–496, https://doi.org/10.1039/C6TA06733F.
[15] J. Lee, S. Kim, J. Yoon, Rocking chair desalination battery based on prussian blue electrodes, ACS Omega 2 (4) (2017) 1653–1659, https://doi.org/10.1021/acsomega.6b00526.

[16] L. Guo, R. Mo, W. Shi, Y. Huang, Z.Y. Leong, M. Ding, F. Chen, H.Y. Yang, A prussian blue anode for high performance electrochemical deionization promoted by the faradaic mechanism, Nanoscale 9 (2017) 13305–13312, https://doi.org/10.1039/C7NR03579A.
[17] T. Kim, C.A. Gorski, B.E. Logan, Ammonium removal from domestic wastewater using selective battery electrodes, Environ. Sci. Technol. Lett. 5 (9) (2018) 578–583, https://doi.org/10.1021/acs.estlett.8b00334.
[18] J. Lee, S. Kim, C. Kim, J. Yoon, Hybrid capacitive deionization to enhance the desalination performance of capacitive techniques, Energ. Environ. Sci. 7 (2014) 3683–3689, https://doi.org/10.1039/C4EE02378A.
[19] C. Zhao, X. Lv, J. Li, T. Xie, Y. Qi, W. Chen, Manganese oxide nanoparticles decorated ordered mesoporous carbon electrode for capacitive deionization of brackish water, J. Electrochem. Soc. 164 (13) (2017) E505, https://doi.org/10.1149/2.0141714jes.
[20] W. Peng, W. Wang, G. Han, Y. Huang, Y. Zhang, Fabrication of 3D flower-like MoS2/graphene composite as high-performance electrode for capacitive deionization, Desalination 473 (2020) 114191, https://doi.org/10.1016/j.desal.2019.114191.
[21] T.K.A. Nguyen, T.-H. Wang, R. an Doong, Architectures of flower-like MoS2 nanosheet coated N-doped carbon sphere electrode materials for enhanced capacitive deionization, Desalination 540 (2022) 115979, https://doi.org/10.1016/j.desal.2022.115979.
[22] E.R. Halabaso, J.W.L. Salvacion, E.P. Kuncoro, R.-A. Doong, Highly efficient capacitive deionization of brackish water with manganese vanadate nanorod decorated reduced graphene oxide electrode, Environ. Sci.: Nano 8 (2021) 2844–2854, https://doi.org/10.1039/D1EN00514F.
[23] E.R. Halabaso, P. Somnath Dayma, J.W.L. Salvacion, R. an Doong, Copper tungstate deposited reduced graphene oxide nanocomposite for highly efficient capacitive deionization, J. Electroanal. Chem. 938 (2023) 117441, https://doi.org/10.1016/j.jelechem.2023.117441.
[24] Y. Oren, Capacitive deionization (CDI) for desalination and water treatment — past, present and future (a review), Desalination 228 (1–3) (2008) 10–29, https://doi.org/10.1016/j.desal.2007.08.005.
[25] M.E. Suss, S. Porada, X. Sun, P.M. Biesheuvel, J. Yoon, V. Presser, Water desalination via capacitive deionization: what is it and what can we expect from it? Energ. Environ. Sci. 8 (8) (2015) 2296–2319, https://doi.org/10.1039/c5ee00519a.
[26] H. Kim, S. Kim, B. Lee, V. Presser, C. Kim, Emerging frontiers in multichannel membrane capacitive deionization: recent advances and future prospects, Langmuir 40 (9) (2024) 4567–4578, https://doi.org/10.1021/acs.langmuir.3c03648.
[27] S.-i. Jeon, H.-r. Park, J.-g. Yeo, S. Yang, C.H. Cho, M.H. Han, D.K. Kim, Desalination via a new membrane capacitive deionization process utilizing flow-electrodes, Energ. Environ. Sci. 6 (5) (2013) 1471, https://doi.org/10.1039/c3ee24443a.
[28] B. Kastening, T. Boinowitz, M. Heins, Design of a slurry electrode reactor system, J. Appl. Electrochem. 27 (1997) 147–152, https://doi.org/10.1023/A:1018443705541.
[29] V. Presser, C.R. Dennison, J. Campos, K.W. Knehr, E.C. Kumbur, Y. Gogotsi, The electrochemical flow capacitor: a new concept for rapid energy storage and recovery, Adv. Energy Mater. 2 (7) (2012) 895–902, https://doi.org/10.1002/aenm.201100768.
[30] K.B. Hatzell, J. Eller, S.L. Morelly, M.H. Tang, J. Alvarez, Y. Gogotsi, Direct observation of active material interactions in flowable electrodes using X-ray tomography, Faraday Discuss. (2017) 511–524, https://doi.org/10.1039/c6fd00243a.
[31] Y. Gendel, A. Rommerskirchen, O. David, M. Wessling, Batch mode and continuous desalination of water using flowing carbon deionization (FCDI) technology, Electrochem. Commun. 46 (2014) 152–156, https://doi.org/10.1016/j.elecom.2014.06.004.
[32] S. Porada, D. Weingarth, H.V. Hamelers, M. Bryjak, V. Presser, P.M. Biesheuvel, Carbon flow electrodes for continuous operation of capacitive deionization and capacitive mixing energy generation, J. Mat. Chem. A 2 (24) (2014) 9313–9321, https://doi.org/10.1039/C4TA01783H.
[33] C. Zhang, J. Ma, L. Wu, J. Sun, L. Wang, T. Li, T.D. Waite, Flow electrode capacitive deionization (FCDI): recent developments, environmental applications, and future perspectives, Environ. Sci. Technol. 55 (2021) 4243–4267, https://doi.org/10.1021/acs.est.0c06552.
[34] M.B. Dixit, D. Moreno, X. Xiao, M.C. Hatzell, K.B. Hatzell, Mapping charge percolation in flowable electrodes used in capacitive deionization, ACS Materials Lett. 1 (1) (2019) 71–76, https://doi.org/10.1021/acsmaterialslett.9b00106.
[35] N. Kim, J. Park, Y. Cho, C.-Y. Yoo, Comprehensive electrochemical impedance spectroscopy study of flow-electrode capacitive deionization cells, Environ. Sci. Technol. 57 (23) (2023) 8808–8817, https://doi.org/10.1021/acs.est.3c01619.
[36] M.C. Padligur, C.J. Linnartz, S. Zimmer, J. Linkhorst, M. Wessling, Coupled optical-electric monitoring of charge percolation events in carbon flow-electrodes, Chem. Eng. J. (2024) 148749, https://doi.org/10.1016/j.cej.2024.148749.
[37] K.B. Hatzell, M.C. Hatzell, K.M. Cook, M. Boota, G.M. Housel, A. McBride, E. C. Kumbur, Y. Gogotsi, Effect of oxidation of carbon material on suspension electrodes for flow electrode capacitive deionization, Environ. Sci. Technol. 49 (5) (2015) 3040–3047, https://doi.org/10.1021/es5055989.
[38] K. Tang, S. Yiacoumi, Y. Li, C. Tsouris, Enhanced water desalination by increasing the electroconductivity of carbon powders for high-performance flow-electrode capacitive deionization, ACS Sustain. Chem. Eng. 7 (1) (2019) 1085–1094, https://doi.org/10.1021/acssuschemeng.8b04746.
[39] I. Hwang, D. Lee, Y. Jung, K. Park, Y.-G. Jung, D. Kim, G.-H. Cho, S.-i. Jeon, Y.-k. Byeun, U. Paik, S. Yang, T. Song, Cross effect of surface area and electrical conductivity for carbonaceous materials in flow-electrode capacitive mixing (F-CapMix) and flow-electrode capacitive deionization (FCDI): solid-like behavior of flow-electrode, ACS Sustain. Chem. Eng. 9 (40) (2021) 13514–13525, https://doi.org/10.1021/acssuschemeng.1c04419.
[40] G. Folaranmi, M. Tauk, M. Bechelany, P. Sistat, M. Cretin, F. Zaviska, Investigation of fine activated carbon as a viable flow electrode in capacitive deionization, Desalination 525 (2022) 115500, https://doi.org/10.1016/j.desal.2021.115500.
[41] J. Wang, Z. Shi, J. Fang, B. Chu, N. Li, L. Shui, G. Wang, F. Chen, The optimized flow-electrode capacitive deionization (fcdi) performance by zif-8 derived nanoporous carbon polyhedron, Sep. Purif. Technol. 281 (2022) 119345, https://doi.org/10.1016/j.seppur.2021.119345.
[42] W. Zhang, W. Xue, K. Xiao, C. Visvanathan, J. Tang, L. Li, Selection and optimization of carbon-based electrode materials for flow-electrode capacitive deionization, Sep. Purif. Technol. 315 (2023) 123649, https://doi.org/10.1016/j.seppur.2023.123649.
[43] L. Yan, S. Issaka Alhassan, H. Gang, B. Wu, D. Wei, Y. Cao, P. Chen, H. Wang, Enhancing charge transfer utilizing ternary composite slurry for high-efficient flow-electrode capacitive deionization, Chem. Eng. J. 468 (2023) 143413, https://doi.org/10.1016/j.cej.2023.143413.
[44] S. Yang, H.-r. Park, J. Yoo, H. Kim, J. Choi, M.H. Han, D.K. Kim, Plate-shaped graphite for improved performance of flow-electrode capacitive deionization, J. Electrochem. Soc. 164 (13) (2017) E480, https://doi.org/10.1149/2.1551713jes.
[45] B. Akuzum, P. Singh, D.A. Eichfeld, L. Agartan, S. Uzun, Y. Gogotsi, E.C. Kumbur, Percolation characteristics of conductive additives for capacitive flowable (semi-solid) electrodes, ACS Appl. Mater. Interfaces 12 (5) (2020) 5866–5875, https://doi.org/10.1021/acsami.9b19739.
[46] Z. Wang, Y. Hu, Q. Wei, W. Li, X. Liu, F. Chen, Enhanced desalination performance of a flow-electrode capacitive deionization system by adding vanadium redox couples and carbon nanotubes, J. Phys. Chem. C 125 (2) (2021) 1234–1239, https://doi.org/10.1021/acs.jpcc.0c09058.
[47] J. Ma, D. He, W. Tang, P. Kovalsky, C. He, C. Zhang, T.D. Waite, Development of redox-active flow electrodes for high-performance capacitive deionization, Environ. Sci. Technol. 50 (24) (2016) 13495–13501, https://doi.org/10.1021/acs.est.6b03424.
[48] L. Luo, Q. He, D. Yi, D. Zu, J. Ma, Y. Chen, Indirect charging of carbon by aqueous redox mediators contributes to the enhanced desalination performance in flow-electrode cdi, Water Res. 220 (2022) 118688, https://doi.org/10.1016/j.watres.2022.118688.
[49] S. Mani, B. Thangapandi, P. Elangovan, A. Prakash, R. Subbaiah, S. Vasudevan, M. Rajendran, New insights into the performance analysis of flow-electrode capacitive deionization using ferri/ferrocyanide redox couples for continuous water desalination, Chem. Eng. J. 480 (2024) 147887, https://doi.org/10.1016/j.cej.2023.147887.
[50] N.H. Freire, C.J. Linnartz, L.A. Montoro, V.S. Ciminelli, M. Wessling, Flow electrode capacitive deionization with iron-based redox electrolyte, Desalination 578 (2024) 117313, https://doi.org/10.1016/j.desal.2024.117313.
[51] J. Chang, F. Duan, H. Cao, K. Tang, C. Su, Y. Li, Superiority of a novel flow-electrode capacitive deionization (FCDI) based on a battery material at high applied voltage, Desalination 468 (2019) 114080, https://doi.org/10.1016/j.desal.2019.114080.
[52] Y. Xu, F. Duan, Y. Li, H. Cao, J. Chang, H. Pang, J. Chen, Enhanced desalination performance in asymmetric flow electrode capacitive deionization with nickel hexacyanoferrate and activated carbon electrodes, Desalination 514 (2021) 115172, https://doi.org/10.1016/j.desal.2021.115172.
[53] A. Heidarian, S.C. Cheung, G. Rosengarten, The effect of flow rate and concentration on the electrical conductivity of slurry electrodes using a coupled computational fluid dynamic and discrete element method (CFD–DEM) model, Electrochem. Commun. 126 (2021) 107017, https://doi.org/10.1016/j.elecom.2021.107017.
[54] C.R. Dennison, M. Beidaghi, K.B. Hatzell, J.W. Campos, Y. Gogotsi, Effects of flow cell design on charge percolation and storage in the carbon slurry electrodes of electrochemical flow capacitors, J. Power Sources 247 (2014) 489–496, https://doi.org/10.1016/j.jpowsour.2013.08.101.
[55] T. Wang, Z. Zhang, Z. Gu, C. Hu, J. Qu, Electron transfer of activated carbon to anode excites and regulates desalination in flow electrode capacitive deionization, Environ. Sci. Technol. 57 (6) (2023) 2566–2574, https://doi.org/10.1021/acs.est.2c09506.
[56] A. Rommerskirchen, Y. Gendel, M. Wessling, Single module flow-electrode capacitive deionization for continuous water desalination, Electrochem. Commun. 60 (2015) 34–37, https://doi.org/10.1016/j.elecom.2015.07.018.
[57] S.K. Patel, M. Qin, W.S. Walker, M. Elimelech, Energy efficiency of electro-driven brackish water desalination: Electrodialysis significantly outperforms membrane capacitive deionization, Environ. Sci. Technol. 54 (6) (2020) 3663–3677, https://doi.org/10.1021/acs.est.9b07482.
[58] J. Ma, C. Zhang, F. Yang, X. Zhang, M.E. Suss, X. Huang, P. Liang, Carbon black flow electrode enhanced electrochemical desalination using single-cycle operation, Environ. Sci. Technol. 54 (2) (2020) 1177–1185, https://doi.org/10.1021/acs.est.9b04823.
[59] C. He, B. Lian, J. Ma, C. Zhang, Y. Wang, H. Mo, T.D. Waite, Scale-up and modelling of flow-electrode CDI using tubular electrodes, Water Res. 203 (2021) 117498, https://doi.org/10.1016/j.watres.2021.117498.

[60] J. Ma, J. Ma, C. Zhang, J. Song, W. Dong, T.D. Waite, Flow-electrode capacitive deionization (FCDI) scale-up using a membrane stack configuration, Water Res. 168 (2020) 115–186, https://doi.org/10.1016/j.watres.2019.115186.
[61] S. Yang, S.-i. Jeon, H. Kim, J. Choi, J.-g. Yeo, H.-r. Park, D.K. Kim, Stack design and operation for scaling up the capacity of flow-electrode capacitive deionization technology, ACS Sustain. Chem. Eng. 4 (8) (2016) 4174–4180, https://doi.org/10.1021/acssuschemeng.6b00689.
[62] N. Köller, L. Mankertz, S. Finger, C.J. Linnartz, M. Wessling, Towards pilot scale flow-electrode capacitive deionization, Desalination (2023) 117096, https://doi.org/10.1016/j.desal.2023.117096.
[63] A. Hermann, T. Chaudhuri, P. Spagnol, Bipolar plates for PEM fuel cells: a review, Int. J. Hydrogen Energy 30 (12) (2005) 1297–1302, https://doi.org/10.1016/j.ijhydene.2005.04.016.
[64] H. Teuku, I. Alshami, J. Goh, M.S. Masdar, K.S. Loh, Review on bipolar plates for low-temperature polymer electrolyte membrane water electrolyzer, Int. J. Energy Res. 45 (15) (2021) 20583–20600, https://doi.org/10.1002/er.7182.
[65] L. Xu, Y. Mao, Y. Zong, D. Wu, Scale-up desalination: membrane-current collector assembly in flow-electrode capacitive deionization system, Water Res. 190 (2021) 116782, https://doi.org/10.1016/j.watres.2020.116782.
[66] L. Xu, Y. Mao, Y. Zong, S. Peng, X. Zhang, D. Wu, Membrane-current collector-based flow-electrode capacitive deionization system: a novel stack configuration for scale-up desalination, Environ. Sci. Technol. 55 (2021) 13286–13296, https://doi.org/10.1021/acs.est.1c03829.
[67] X. Zhang, H. Zhou, Z. He, H. Zhang, H. Zhao, Flow-electrode capacitive deionization utilizing three-dimensional foam current collector for real seawater desalination, Water Res. 220 (2022) 118642, https://doi.org/10.1016/j.watres.2022.118642.
[68] X. Zhang, M. Pang, Y. Wei, F. Liu, H. Zhang, H. Zhou, Three-dimensional titanium mesh-based flow electrode capacitive deionization for salt separation and enrichment in high salinity water, Water Res. 251 (2024) 121147, https://doi.org/10.1016/j.watres.2024.121147.
[69] R. Chen, X. Deng, C. Wang, J. Du, Z. Zhao, W. Shi, J. Liu, F. Cui, A newly designed graphite-polyaniline composite current collector to enhance the performance of flow electrode capacitive deionization, Chem. Eng. J. 435 (2022) 134845, https://doi.org/10.1016/j.cej.2022.134845.
[70] Y. Li, J. Ma, M. Yu, J. Niu, J. Gu, M. Chen, P. Zhang, J. Zhang, C. Liu, Carbon felt (CF) acted as an “ionic capacitor” to enhance flow electrode capacitive deionization (FCDI) desalination performance, Desalination 575 (2024) 117341, https://doi.org/10.1016/j.desal.2024.117341.
[71] H. Saif, T. Gebregeorgis, J. Crespo, S. Pawlowski, The influence of flow electrode channel design on flow capacitive deionization performance: experimental and CFD modelling insights, Desalination 578 (2024) 117452, https://doi.org/10.1016/j.desal.2024.117452.
[72] C.J. Linnartz, A. Rommerskirchen, J. Walker, J. Plankermann-Hajduk, N. Köller, M. Wessling, Membrane-electrode assemblies for flow-electrode capacitive deionization, J. Membr. Sci. 605 (2020) 118095, https://doi.org/10.1016/j.memsci.2020.118095.
[73] S. Dhakate, S. Sharma, M. Borah, R. Mathur, T. Dhami, Expanded graphite-based electrically conductive composites as bipolar plate for PEM fuel cell, Int. J. Hydrogen Energy 33 (23) (2008) 7146–7152, https://doi.org/10.1016/j.ijhydene.2008.09.004.
[74] A. Rommerskirchen, M. Alders, F. Wiesner, C.J. Linnartz, A. Kalde, M. Wessling, Process model for high salinity flow-electrode capacitive deionization processes with ion-exchange membranes, J. Membr. Sci. 616 (2020) 118614, https://doi.org/10.1016/j.memsci.2020.118614.
[75] A. Celzard, J.F. Marêché, G. Furdin, S. Puricelli, Electrical conductivity of anisotropic expanded graphite-based monoliths, J. Phys. D Appl. Phys. 33 (23) (2000) 3094, https://doi.org/10.1088/0022-3727/33/23/313.
[76] C. Jiang, Y. Wang, Z. Zhang, T. Xu, Electrodialysis of concentrated brine from ro plant to produce coarse salt and freshwater, J. Membr. Sci. 450 (2014) 323–330, https://doi.org/10.1016/j.memsci.2013.09.020.
[77] B. Sun, M. Zhang, S. Huang, J. Wang, X. Zhang, Limiting concentration during batch electrodialysis process for concentrating high salinity solutions: a theoretical and experimental study, Desalination 498 (2021) 114793, https://doi.org/10.1016/j.desal.2020.114793.
[78] X. Zhang, J. Zhou, H. Zhou, H. Zhang, H. Zhao, Enhanced desalination performance by a novel archimedes spiral flow channel for flow-electrode capacitive deionization, ACS EST Engg. 2 (7) (2022) 1250–1259, https://doi.org/10.1021/acsestengg.1c00445.
[79] L. Yan, J. Annor Asare, B. Wu, H. Gang, D. Wei, Y. Cao, P. Chen, H. Wang, L. Huang, A hexagonal honeycomb-shaped flow channel for high-efficient desalination and flowability in flow-electrode capacitive deionization, ACS EST, Water 3 (8) (2023) 2753–2764, https://doi.org/10.1021/acsestwater.3c00242.
[80] J. Ma, X. Wang, Y. Bian, C. Zhang, C. Liu, J. Niu, J. Zhang, G. Shen, J. Liu, Novel current collector with mosquito-repellent incense-shaped channel of flow electrode capacitive deionization, ACS Sustain. Chem. Eng. 10 (15) (2022) 4818–4821, https://doi.org/10.1021/acssuschemeng.2c00442.